Journal of Applied Geophysics 229 (2024) 105493

Contents lists available at ScienceDirect

Journal of Applied Geophysics

journal homepage: www.elsevier.com/locate/jappgeo

Comparison of machine learning and electrical resistivity arrays to inverse modeling for locating and characterizing subsurface targets

Ahsan Jamil [a], Dale F. Rucker [b], Dan Lu [c], Scott C. Brooks [d], Alexandre M. Tartakovsky [e], Huiping Cao [f], Kenneth C. Carroll [a,*]

[a] Department of Plant and Environmental Sciences, New Mexico State University, Las Cruces, NM 88003, USA
[b] hydroGEOPHYSICS, Inc., 2302 N Forbes Blvd, Tucson, AZ 85745, USA
[c] Computational Sciences and Engineering Division, Oak Ridge National Laboratory, Oak Ridge, TN 37830, USA
[d] Environmental Sciences Division, Oak Ridge National Laboratory, P.O. Box 2008, MS 6038, Oak Ridge, TN 37831-6038, USA
[e] Department of Civil and Environmental Engineering, University of Illinois at Urbana-Champaign, Urbana, IL 61801, USA
[f] Department of Computer Sciences, New Mexico State University, Las Cruces, NM 88003, USA

ARTICLE INFO

Keywords:
Geophysics
Electrical resistivity
Neural networks
Machine learning
Random forests
Boosting

ABSTRACT

This study evaluates the performance of multiple machine learning (ML) algorithms and electrical resistivity (ER) arrays for inversion with comparison to a conventional Gauss-Newton numerical inversion method. Four different ML models and four arrays were used for the estimation of only six variables for locating and characterizing hypothetical subsurface targets. The combination of dipole-dipole with Multilayer Perceptron Neural Network (MLP-NN) had the highest accuracy. Evaluation showed that both MLP-NN and Gauss-Newton methods performed well for estimating the matrix resistivity while target resistivity accuracy was lower, and MLP-NN produced sharper contrast at target boundaries for the field and hypothetical data. Both methods exhibited comparable target characterization performance, whereas MLP-NN had increased accuracy compared to Gauss-Newton in prediction of target width and height, which was attributed to numerical smoothing present in the Gauss-Newton approach. MLP-NN was also applied to a field dataset acquired at U.S. DOE Hanford site.

1. Introduction

Among the various geophysical methods available, electrical resistivity (ER) is one of the most common for geologic and hydrologic applications (Loke et al., 2013). This method operates on the principle of utilizing differences in electric potential for identifying subsurface materials by injecting an electric current into the subsurface through galvanic contact between positive and negative electrodes (Rucker et al., 2021a). Resultant difference in electric potential, specifically the voltage, is then measured between two or more additional electrodes (Rucker et al., 2021a; Singha et al., 2022). The broad spectrum of applications for the ER method encompasses environmental and engineering disciplines such as hydrological surveying (Pearson et al., 2022) and mining (LaBrecque et al., 1996). They have been extensively used for determining the thickness of layered media and mapping geological environments of aquifers (Riwayat et al., 2018; Rucker et al., 2021a). Application of ER also includes locating and delineating geometric attributes of target zones, or anomalous bodies, of differing resistivity with respect to the surrounding domain or subsurface matrix. ER can be used to detect both conductive targets such as underground storage tanks or tunnels (Pang et al., 2022) and resistive targets including characterizing spills of non-aqueous phase liquid organic contaminants (Kang et al., 2018).

Inversion of ER data is a crucial step in processing and interpreting measurements for accurate reconstruction of subsurface material properties, as geologic interpretations derived from observed geophysical data can often be misleading and inadequate in capturing the intricate characteristics of subsurface heterogeneity. Inverse modeling refers to the determination of the characteristics of a system (i.e., calibration or parameter estimation), based on comparison between observations and modeling results (Sidrane et al., 2022; Yeh et al., 2015). This is commonly completed via the inverse approach, by iteratively minimizing the difference between the observations and model estimated values (an objective function), usually in a least-squares approach.

* Corresponding author.
E-mail addresses: ahsan@nmsu.edu (A. Jamil), lud1@ornl.gov (D. Lu), brookssc@ornl.gov (S.C. Brooks), amt1998@illinois.edu (A.M. Tartakovsky), hcao@nmsu.edu (H. Cao), kccarr@nmsu.edu (K.C. Carroll).

https://doi.org/10.1016/j.jappgeo.2024.105493
Received 9 November 2023; Received in revised form 12 August 2024; Accepted 12 August 2024
Available online 13 August 2024

Nonidentifiability exists when more than one set of parameter values lead the model to reproduce the observed data within an allowable difference (Tsai et al., 2022), which is due to the ill-posed nature of the inverse modeling (Arridge et al., 2019). Geophysical inverse problems are often ill-posed, nonunique, and nonlinear problems (Hayley et al., 2011) implying that even minor inaccuracies in data can result in substantial discrepancies in the model parameters, which illustrates some of the accuracy limitations for the industry standard numerical inversion method. For instance, if a geophysical inverse problem involves estimating the subsurface properties of a rock formation, the ill-posed nature of the problem implies that slight errors or noise in the collected data can lead to significant variations in the predicted rock properties. Similarly, in the context of groundwater modeling, the nonuniqueness of hydrogeological inverse problems suggests that small uncertainties in the measured data can produce large differences in the estimated aquifer characteristics, such as permeability or water storage capacity. For the ER method, observed or measured apparent ER is transformed into an estimate of the true resistivity value through a geophysical numerical inversion (Loke et al., 2020). A contrast between materials of differing resistivity helps to characterize different meta-attributes of targets including size, width, height, shape, and location.

Geophysical inversion methods and machine learning (ML) techniques both provide solutions to the inverse problem. Geophysical inversion is typically founded upon models representing physical processes that govern the recorded data, but ML represents a data-centric statistical methodology aimed at resolving ill-posed inverse problems through the exploitation of vast amounts of data through pattern matching (Kim and Nakata, 2018). Several recent studies have used ML techniques for ER inversion (Liu et al., 2020a) by proposing to build a correspondence between measurements of apparent resistivity data and the true resistivity spatial distributions mostly by utilizing convolutional neural networks (CNN) (Aleardi et al., 2021; Liu et al., 2020b; Liu et al., 2022; Vu and Jardani, 2021; Wilson et al., 2022). Another study by Liu et al. (2020b) demonstrated that the use of adaptive convolutional networks represents a promising approach for resolving the ER inverse problem, as it utilizes convolutional kernels specifically optimized for ER inversion. Another approach with fuzzy deep wavelet neural network inversion was introduced by Dong et al. (2022), which uses an optimized accelerated hybrid learning algorithm to invert resistivity data. Furthermore, Jiang et al. (2020) proposed a multi-output, support vector regression as a nonlinear inversion method with limited ER learning samples to solve the 2D ER inversion problem, but generally ER inversion research has mostly focused on using the CNN class of ML methods (Aleardi et al., 2021; Liu et al., 2020a; Liu et al., 2020b; Liu et al., 2022; Vu and Jardani, 2021; Wilson et al., 2022). Despite the significant advancements and interest in using ML for ER inversion, there is a noticeable gap in previous research regarding a comprehensive comparison and evaluation of contemporary ML algorithms and the quantification of their performance with different kinds of ER geophysical arrays. This constitutes a major overlooked aspect since different ER array configurations have variabilities in resolution, acquisition efficiency, depth of signal penetration, or signal-to-noise ratio (Rucker and Glaser, 2015).

Since prior investigations have not compared a wide range of ML methods for a set of ER arrays as applied to ER data inversion, the objective of this study was to assess the ability of ML methods to reconstruct the geometry and determine the location of an anomalous target body, defined as a medium of contrasting resistivity relative to the surrounding domain, in a 2D profile. To decrease development time and training requirements, we focused on only predicting six key parameters, which are target characteristics for locating and characterizing buried targets. These six target-characterization predictors included target location centroid in x and z directions (i.e., lateral and vertical center positions), width of the target body, height of the target body, target resistivity, and the matrix resistivity (i.e., resistivity of the surrounding environment). This approach is similar to previous numerical ER inversion studies that examined domains with homogeneous regions separated by a sharp boundary (Hiskiawan et al., 2023; Olayinka and Yaramanci, 2000; Shamara et al., 2023). Several ER arrays were compared using multiple ML methods to identify the combination with the best target prediction capability, and then the best-performing ML method and ER array was compared with an industry standard inverse modeling approach using the Gauss-Newton method. ML algorithms were also applied to a field dataset that was acquired over a known plume of liquid waste disposed in sand and silt matrix at the Hanford Site in central Washington State, USA. The area is well studied, and the waste plume has been previously characterized (Rucker and Glaser, 2015; Rucker et al., 2013).

2. Materials and methods

A systematic approach to developing and evaluating ML for ER inversion was used, starting from forward modeling to generate synthetic data, and concluding with the application of the best-performing algorithm to real-world data and reporting the results (Fig. 1). ML model development and implementation stages included preparation of synthetic datasets, hyperparameter selection, data pre-processing, ML training/testing, evaluating the prediction results for comparison to the test dataset, application to a field dataset, and the uncertainty quantification of the model.

2.1. Software and packages used

Software packages and Python codes used in this study are listed in Table 1. Scikit-learn, a Python library, was used in this study for its ability to integrate a diverse range of state-of-the-art ML algorithms. The library is suitable for addressing both medium-scale supervised and unsupervised problems (Pedregosa et al., 2011). Application of other software packages listed in Table 1 are addressed in the following sections.

2.2. Preparation of synthetic dataset

ER modeling code, ResIPy (Blanchy et al., 2020) was used to generate 2D ER training and testing data by forward modeling hypothetical scenarios with known resistivity distributions (Fig. 2). ResIPy uses the finite element method (Kosloff and Baysal, 1982) with no flux (Neumann) boundary conditions. ResIPy was chosen for its user-friendly interface, specificity to ER modeling, reliance on established methodology, and active development community. The output of the forward modeling process was the calculation of apparent resistivity (Fig. 2b), which would be analogous to a field acquisition survey except the true resistivity distribution was known for the hypothetical scenarios.

The hypothetical scenario series had a model domain of 120 × 40 m (m) in size with a single embedded target body within a surrounding matrix of differing material property (i.e., resistivity). This is a simple two-domain version of heterogeneity that does not capture the typical extent of subsurface spatial variability but is a common conceptualization for locating individual buried targets such as underground storage tanks or tunnels, waste spills, geologic lens, ore deposits, underground mines, or karst-cave features. An example of the model mesh and domain is illustrated in Fig. 2a, and the figure also shows arrows indicating the inverse modeling process used to determine the resistivity material property distributions from the apparent resistivity measurement distribution with the other arrow showing the forward model approach for comparison. Here, we only include one target to illustrate the approach, but additional targets, or different shapes of targets, could be added depending on site-specific conditions and survey goals. The location, size, and dimensions of the target body varied over a wide range for each of the six target characteristics for locating and characterizing buried targets. Model setup included a surface array of 25 electrodes spaced 5 m apart for each of the four geophysical array

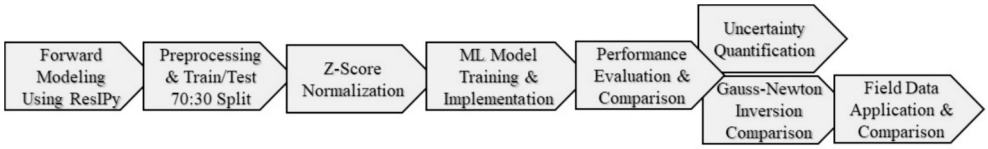

Fig. 1. Workflow of model development, implementation, and comparisons with numerical inversion methods.

Table 1
Software and/or source codes used in this study.

No.	Module	Programming Language/ Developer	Purpose	URL
1	Scikit-learn v1.0.2	Python	ML implementation	https://scikit-learn.org/
2	ResIPy v 3.4.1	Python API	For forward modeling of ERT data	https://gitlab.com/hkex/resipy
3	RES2DINVx64 v4.05	Aarhus Geosoftware	For inverse modeling /validation and comparison	https://www.aarhusgeosoftware.dk/res2dinv
4	Surfer v14.0	Golden Software	Contouring, plotting and visualizing ERT data	https://www.goldensoftware.com/products/surfer
5	Pi3nn	Liu et al. (2021)	Uncertainty quantification of model	https://github.com/liusiyan/UQnet/tree/master/pi3nn
6	NumPy v 1.21.5	Oliphant (2007)	Numerical computing/ random number generation	https://www.NumPy.org

configurations. Forward modeling training/testing data set generation for ML inversion evaluation included the performance comparison of Alt3 Wenner (Cubbage et al., 2017), Wenner-Schlumberger, Dipole-Dipole, and gradient arrays (Rucker et al., 2021b), which are four different and commonly used ER arrays.

The hypothetical scenarios included ranges of the randomly generated values for each target variable used to modify the model material property distributions for the forward modeling scenarios (Table 2). The values for each variable were generated by using the random number generator in the NumPy Python library (Oliphant, 2007), and the ranges were designed to span typical values found in ER surveys. This library provides robust capabilities for performing computations on extensive multidimensional arrays and offers an expansive collection of mathematical functions (Van Der Walt et al., 2011). Equal sample sizes of 20,000 scenarios (Data 1) were generated for each of the four arrays, resulting in a total of 80,000 forward model data instances. Both conductive and resistive target scenarios were considered in equal proportion (10,000 data instances each) to avoid bias toward a particular target type. The minimum ratio between target and matrix resistivity difference was set to 2:1 to ensure contrast between two heterogenous mediums. Another batch of 20,000 scenarios (Data 2) of the best performing array configuration was generated with extended ranges of matrix and target resistivity to assess the feasibility of model application on real world data that included larger resistivity values.

Data normalization is another important technique in data preprocessing that rescales variables to a common scale, allowing for fair comparisons and reducing impact of variables with different units or scales on the analysis results (Gómez-Escalonilla et al., 2022). Several methods exist for data normalization, for example min-max normalization, z-score normalization, and normalization by decimal scaling (Al Shalabi et al., 2006). *Z*-score normalization was used in this study resulting in data with mean of zero and unit variance. Normalized input features were then used for training all four above mentioned ML algorithms on all four different geophysical array configurations.

The set of forward models were split into a 70:30 training-to-testing ratio, with 14,000 records used for training and 6000 data instances used for testing the algorithms. The decision to use a 70:30 training-to-

Table 2
Ranges for the forward model datasets for six target parameters.

Parameter	Data 1		Data 2	
	Min	Max	Min	Max
Centroid x (meter)	1.5	118.5	1.5	118.5
Centroid z (meter)	−29.5	−2.5	−21.5	−2.5
Width (meter)	1	118	1	118
Height (meter)	1	28	1	20
Matrix resistivity (ohm.meter)	1	1000	1	5000
Target resistivity (ohm.meter)	1	1000	1	5000

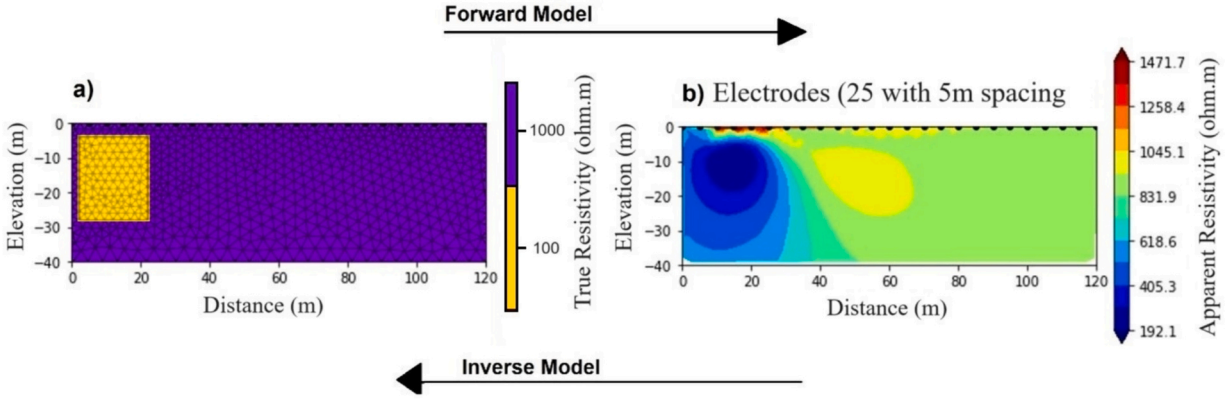

Fig. 2. Conceptual diagram showing inverse and forward resistivity model, a) model mesh and the target body that shows region of contrasting resistivity with respect to the matrix, and b) shows electrode spacing on upper land surface boundary and spatially variable apparent resistivity distribution from forward model solution of electrical injection.

testing ratio was based on standard practices, dataset size and complexity, and reference from prior related studies (Chojnicki et al., 2022). Independent data (input parameters) were the 2D spatial distribution of apparent resistivity values obtained from the forward modeling, upwards of 250 values per array. The dependent data for ML prediction was based on the six target characteristics. Limiting prediction to a small set of variables that describe a target's attributes achieves the goal of locating and defining the target spatial extent with a significant reduction in prediction variables compared to full 2D prediction of spatial distribution of resistivity properties. Based on the parameter estimation accuracy, comparison of results for the best-performing ML method and geophysical array with the Gauss-Newton method (using the industry standard RES2DINV model) was performed to evaluate the comparative proficiency of ML versus conventional numerical inversion techniques. To accomplish this task, results of Gauss-Newton inversed 2D spatial distribution of true resistivity were evaluated to determine the six target parameters for comparison with the statistically best performing ML algorithm. A thresholding technique was implemented using Surfer 14.0 software to identify the target zone boundary and delineate the six target characterization variables for comparison with ML model results. Thresholding involved estimation of the two resistivity zone means and calculating the boundary as the midpoint of the difference between the two mean resistivities.

2.3. ML implementation for parameter estimation

An objective of this study was to evaluate ER inversion using a wide range of ML methods. To identify the optimal ML method, performance of four ML algorithms was compared, including Multilayer Perceptron Neural Network (MLP-NN), Extreme Gradient Boosting Regressor (XGBR), Random Forests (RF), and Light Gradient Boosting Machine (LGBM). The choice of ML algorithms allowed for comparison of three very different strategies for the ER inverse problem, and each ML method is unique in architecture and approach. For example, MLP-NN belongs to the family of Deep Neural Networks (which also includes the CNN approach). RF belongs to a family of bagging type of ensemble approaches (Wen and Hughes, 2020). XGBR and LGBM belong to the boosting type of ensemble algorithms (Tran et al., 2021). These four specific ML algorithms were considered for analysis based on a combination of factors such as their widespread usage, proven effectiveness in handling regression tasks, ability to handle complex data patterns, and compatibility with the dataset and research objectives. These algorithms were chosen to ensure a comprehensive comparison across different types of ML methods, providing a well-rounded evaluation of their performance for the ERT inversion problem.

MLP-NN architecture design is contingent upon the selections made regarding objective function, number of hidden layers, and number of hidden nodes in each layer (Ramchoun et al., 2016). First, we chose an MLP-NN regression model with three layers: one input layer, one hidden layer, and one output layer. Hyperparameter selection is important in implementing MLP-NN, because it significantly affects model performance, including its ability to learn, generalize, and make accurate predictions (Sahu et al., 2020). A trial-and-error approach was employed to select the hyperparameters for the MLP-NN model (Table 3). Selected hyperparameters included number of hidden layers, number of nodes in each hidden layer, solver, number of epochs, and activation function. This method involved iteratively training the model with different combinations of hyperparameters and evaluating their performance using the coefficient of correlation (represented by R^2) as evaluation metric. The combination that achieved the best results was then chosen as the final set of hyperparameters for the MLP-NN model. This approach has been widely used, and has been effective in determining optimal hyperparameters for neural network models (Kalliola et al., 2021). We considered 'tanh' and 'ReLU' activation functions during model development (Kunc and Kléma, 2024; Qi et al., 2017). While ReLU helps address the vanishing gradient problem, it is not always the superior choice for all scenarios. Activation functions like 'tanh' have their own advantages, such as being able to capture both positive and negative values, which is beneficial for certain types of data, e.g., for datasets pre-processed with the z-score normalization (Karlik and Olgac, 2011). We decided to use the 'tanh' activation function based on its superior performance over ReLU for this application.

Table 3
Comparison and summary of MLP-NN model performance (R^2) with different hyperparameter configuration where R^2 represents combined coefficient of correlation for six parameters for the test data.

Nodes (single hidden layer)	Activation	Solver	R^2 for test data	Epochs
10	tanh	Adam	0.46	1000
100	tanh	Adam	0.55	1000
1000	tanh	Adam	0.58	2000
10	tanh	lbfgs	0.57	2000
10	tanh	lbfgs	0.60	3000
100	tanh	lbfgs	0.69	2000
100	tanh	lbfgs	0.70	3000
1000	tanh	lbfgs	0.76	3000
1500	tanh	lbfgs	0.79	3000
1500	ReLU	lbfgs	0.76	3000
2000	tanh	lbfgs	0.81	3000
Nodes (2 hidden layers)	Activation	Solver	R^2 for test data	Epochs
2000–2000	tanh	lbfgs	0.80	3000

Table 3 shows that the coefficient of correlation for the predicted parameters using 'tanh' was 0.81, which was higher than the 0.76 obtained using 'ReLU'. Similarly, the optimization solver 'lbfgs' was selected due to its superior performance ($>R^2$) as compared to other contemporary solvers such as 'Adam' as shown in Table 3. The hidden layer was comprised of 2000 nodes, and although parameter estimation was attempted using two hidden layers, this approach resulted in an increase in computational time without improvement in model performance as compared to the single hidden layer (Table 3). Therefore, MLP-NN with a single hidden layer was used for the remainder of this investigation. The size of the MLP-NN output layer was six and the outputs (centroid-x, centroid-z, width, height, matrix resistivity, and target resistivity) are the six feature parameters. The input layer size was ~250 and the inputs were the ~250 apparent resistivity values (corresponding to the number of measurements for the geophysical array).

The second ML algorithm applied for estimating target characterization parameters was RF, a representative of the bagging ensemble approach. RF is a meta-estimator that trains several decision trees on different training dataset samples, using averaging to enhance predictive accuracy and prevent over-fitting (Reading et al., 2015). Two crucial hyperparameters for this algorithm are the number of base estimators and the maximum depth. Based on a trial-and-error approach 1000 estimators and a maximum depth of 100 for the decision tree were selected as hyperparameters. Similar to the MLP-NN, the input data for the RF model was the normalized feature data for the inputs (~250 apparent resistivity values), and the output was also a prediction for each of the six target variables.

Lastly, two regression models from the boosting ensemble approach were implemented, which included the XGBR and the LGBM regressors. XGBR, proposed by Chen and Guestrin (2016), is a boosting technique that creates strong learners through an additive training process and minimizes over-fitting by incorporating model complexity as a regularization term into the cost function (Pham et al., 2020). LGBM-based models are considered faster and more memory-efficient than other methods. LGBM uses 'Gradient One-Side Sampling' method to build trees, retaining only instances with larger gradients and discarding those with smaller gradients, leading to faster training and more accurate gain estimation (Bisht et al., 2022). As with the other ML models, the input data for the XGBR and LGBM models were the ~250 apparent resistivity values and outputs were the six target parameters. Some strengths and limitations of the ML methods used herein are shown in Table 4.

2.4. Uncertainty quantification

Uncertainty quantification (UQ) of models is crucial, as it provides a more complete understanding of the limitations and confidence levels of predictions and decisions, enabling more informed and evidence-based choices. The PI3NN method was developed by Liu et al. (2021) for quantifying ML model prediction uncertainties. The method is computationally efficient, robust, and produces uncertainties consistent with the confidence level (Liu et al., 2023). ML models are data driven, and here we use them to learn the relationship between the ER observation variables and the six unknown parameters based on the forward model simulation scenarios. UQ can help diagnose whether the ML model has learned the right relationship and if it has correctly solved the inverse problem. PI3NN quantifies uncertainty using prediction intervals, which are calculated using three neural networks. We used two prediction interval metrics to evaluate the UQ performance: mean prediction interval width (MPIW); and prediction interval coverage probabilities (PICP). We refer the reader to (Liu et al., 2023) for the details of this UQ approach.

This investigation is important especially when ground truth is unavailable, in that case it is not possible to calculate the prediction error to evaluate performance. For the PI3NN method to quantify the uncertainty, MPIW can be used to evaluate the model estimation accuracy. If the MPIW of the estimated parameters in the test set has similar values (usually in the same magnitude) to the training set, then the ML model has learned the unbiased observation-parameter relationship and the estimation results on the test set can be trusted. Additionally, the ML model estimation can be full of uncertainty associated with the limited training sample size, the uncertain model structure, and model hyperparameter values. It is critical to quantify the influence of these uncertain factors on the parameter estimates. In an accurate UQ at a 95% confidence level, the calculated prediction interval should cover approximately 95% of the data points. PICP was used to measure the accuracy of UQ, where the PICP of test data is calculated as the test data ratio inside the prediction interval to the total number of test data.

2.5. Gauss-Newton Resistivity Inversion

To assess the robustness of ML-predicted inversion, a small subset of forward models were used to generate synthetic ground truth and the parameters (resistivity field) were also estimated by calibration using a standard inversion code RES2DINVx64. Dey and Morrison (1979) presented the 2D electrical resistivity partial differential equations, boundary conditions, discretization, and numerical solution. Borrowing from the descriptions of resistivity inversion by others (Dahlin et al., 2002; Hilbich et al., 2009; Loke and Barker, 1996; Loke and Dahlin, 2002), the equation for the constrained optimization, nonlinear least-squares (i.e., Gauss-Newton method):

$$\left[J_i^T R_d J_i + \left(\lambda_i W^T R_m W\right)\right]\Delta r_i = J_i^T R_d g_i - \left(\lambda_i W^T R_m W\right) r_{i-1} \quad (1)$$

describes the relationship between model parameters and measured data. The model parameters in vector r are the ER values at each discretized cell within the model domain. The optimization procedure marches along a piece-wise linear path on the error surface using a model updating procedure to calculate a Δr_i at iteration i using information about r_{i-1} and the sensitivity matrix, J, containing the partial derivative of data measurements relative to the model parameters. To dampen the effects of noise being amplified through the modeling procedure, a matrix roughness filter (W) and data and model weighting matrices (R_d and R_m, respectively) are used in the algorithm. The remaining parameters include the data misfit vector, g_i, and the spatial dampening factor (λ_i). The optimization procedure objective is to reduce the misfit between measured and modeled apparent resistivity values in a least-squares sense.

Table 4
Summary of strengths and limitations of four ML algorithms.

Algorithm	Strengths	Limitations
MLP-NN	Ability to learn complex non-linear relationships in data	Sensitive to hyperparameter tuning
	Versatility in handling various types of data and feature engineering	Prone to overfitting if the network architecture is too complex or if the dataset is small
RF	Robust against overfitting and able to handle high-dimensional data	Lack of interpretability compared to simpler models
	Effective in capturing non-linear relationships and interactions between features	Computationally expensive during training and prediction, especially for large datasets
XGBR	High predictive accuracy and strong performance in various regression tasks	Sensitive to hyperparameter tuning
	Ability to handle missing data and outliers effectively	Requires careful regularization to avoid overfitting
LGBM	Fast and efficient training and prediction, especially for large datasets	Less interpretability compared to simpler models
	Good handling of high-dimensional data with many features	Requires careful hyperparameter tuning and regularization to prevent overfitting

3. Results and discussion

3.1. Comparison of performance of ML methods for four ER arrays for target delineation

Table 5 presents the median values of dimensionless relative error of the four ML models and for each of the four ER arrays. Medians were considered to reduce the effect of data skewness toward higher values (data distribution for each parameter is shown in Fig. S1 of Supporting Information (SI)). The unitless relative error is a measure of the model prediction accuracy compared to the true values. The relative error was calculated for each of the six predicted target identification parameters by comparison of testing dataset predictions to hypothetical true values. It is calculated as the ratio of the difference between the predicted and true values relative to the true values expressed as:

$$\textit{Relative error} = (|\textit{True value} - \textit{Predicted value}|)/\textit{True value} \quad (2)$$

and standard error of the mean (SEM) was calculated as:

$$\textit{SEM} = \textit{Standard deviation of Median Relative Error}/\sqrt{(\textit{Number of samples})} \quad (3)$$

Among the four ER arrays tested, the dipole-dipole array performed as well as or better than the other arrays for all ML models based on the average median relative error of the six target parameters (Table 5). The dipole-dipole array combined with the MLP-NN model produced the lowest average relative error (0.16 ± 0.06) and the XGBR-Wenner-Schlumberger combination had the highest relative error (0.25 ± 0.07). Among the estimated target parameters, height and target resistivity had the highest relative error for all ML model–ER array combinations. Relative errors for these two parameters were several times, or more, greater than the relative errors associated with the remaining four parameters. ML models were additionally evaluated by taking the arithmetic mean of average median relative errors for each of the four ML groups (Table 5). The MLP-NN model produced the lowest arithmetic mean of relative error (~0.17). This result is also consistent with the strengths of MLP-NN to solve complex non-linear problems (Table 4). In comparison, the highest arithmetic mean of relative error (~0.24) was produced by XGBR method, which was 41% higher than MLP-NN. RF and LGBM models produced errors of ~0.21 and ~ 0.22, respectively. Nevertheless, due to the high within-ML model variance there was no statistically significant difference among ML model mean

Table 5
Performance, as relative error, comparison for ML models and ER arrays for target parameter estimation. The last two columns show the average relative error (standard error of the mean) for each array and each ML method.

ML Model	ER Array	Target Centroid-x	Target Centroid-z	Target Width	Target Height	Matrix Resistivity	Target Resistivity	ER Array Mean (SEM)[a]	ML Model Mean (SEM)[b]
MLP-NN	Alt3 wenner	0.08	0.10	0.17	0.33	0.004	0.41	0.18 (0.16)	0.17 (0.14)
	Dipole-dipole	0.06	0.09	0.15	0.28	0.006	0.38	0.16 (0.14)	
	Gradient	0.07	0.10	0.15	0.29	0.004	0.38	0.17 (0.14)	
	Wenner-Schlumberger	0.06	0.10	0.17	0.31	0.004	0.41	0.18 (0.16)	
RF	Alt3 wenner	0.05	0.16	0.30	0.40	0.003	0.36	0.21 (0.17)	0.21 (0.15)
	Dipole-dipole	0.05	0.14	0.26	0.38	0.003	0.37	0.20 (0.16)	
	Gradient	0.05	0.15	0.26	0.39	0.003	0.37	0.20 (0.16)	
	Wenner-Schlumberger	0.05	0.15	0.30	0.39	0.004	0.37	0.21 (0.17)	
XGBR	Alt3 wenner	0.11	0.18	0.31	0.42	0.01	0.42	0.24 (0.17)	0.24 (0.16)
	Dipole-dipole	0.10	0.16	0.28	0.41	0.01	0.41	0.23 (0.17)	
	Gradient	0.10	0.18	0.30	0.42	0.01	0.42	0.24 (0.17)	
	Wenner-Schlumberger	0.12	0.17	0.33	0.42	0.01	0.43	0.25 (0.17)	
LGBM	Alt3 wenner	0.08	0.16	0.27	0.40	0.01	0.40	0.22 (0.16)	0.22 (0.15)
	Dipole-dipole	0.07	0.13	0.23	0.37	0.01	0.39	0.20 (0.16)	
	Gradient	0.08	0.15	0.24	0.39	0.01	0.40	0.21 (0.16)	
	Wenner-Schlumberger	0.09	0.15	0.31	0.40	0.01	0.42	0.23 (0.17)	

[a] Arithmetic mean of relative errors across the six target parameters within the given array. SEM = standard error of the mean.
[b] Arithemetic mean of all relative errors within the listed ML model.

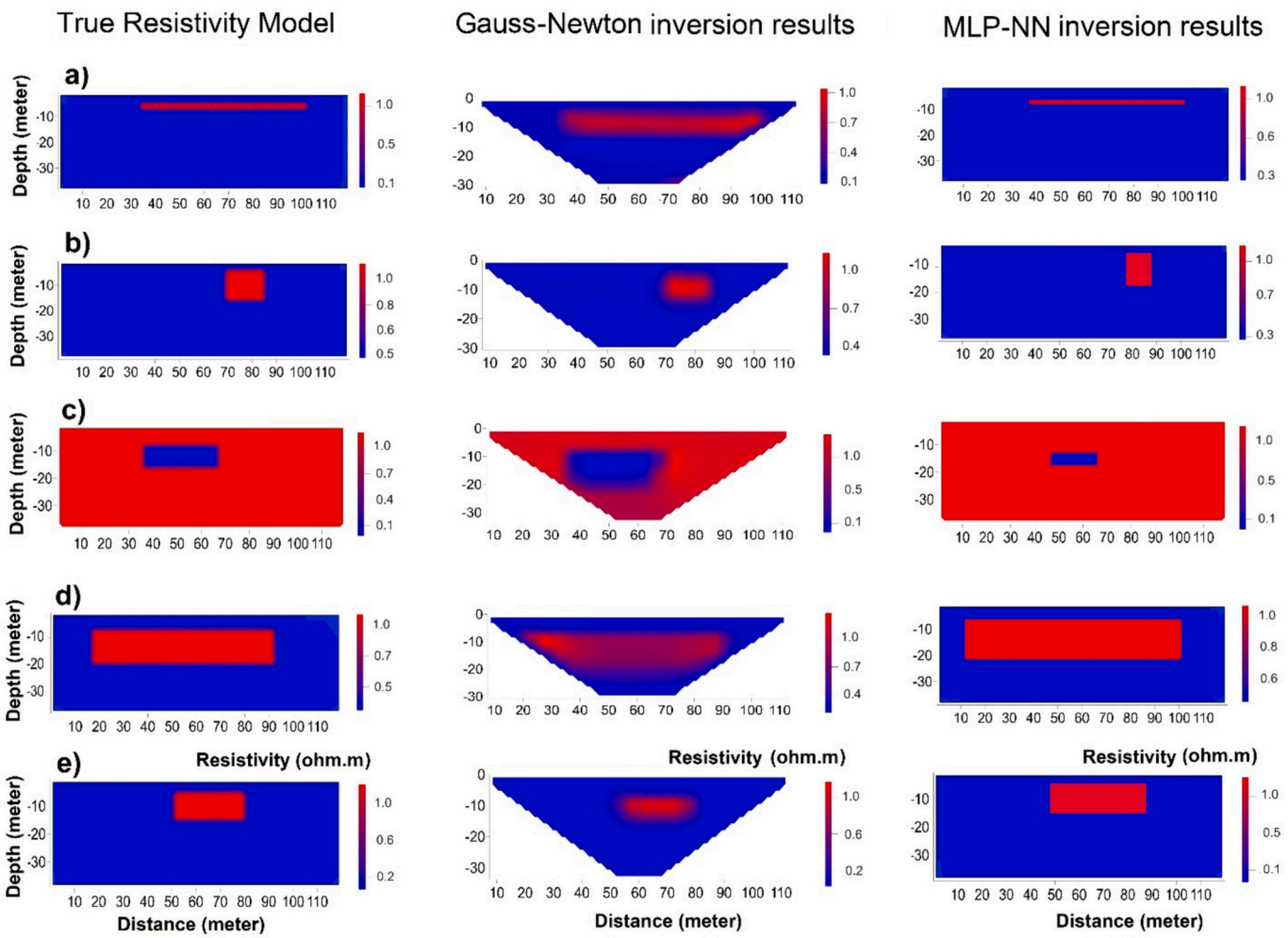

Fig. 3. Comparison between true resistivity model (left column), standard inversion results obtained from Gauss-Newton method (middle column) and MLP-NN inversion results on Dipole-Dipole array (right column) for five representative examples (a-e) of the 30 test cases. Note: resistivity scales were normalized by maximum resistivity for each scenario.

relative errors.

3.2. Comparison of Gauss-Newton numerical inversion and ML-based parameter estimation

Thirty randomly selected scenarios from the MLP-NN ML synthetic dataset (applied with Dipole-Dipole configuration) were used to conduct prediction performance comparison between MLP-NN and Gauss-Newton numerical inverse modeling methods for target-characterization parameter estimation. Five of the thirty scenarios are presented to illustrate the comparison of these methods (Fig. 3). From visual inspection of these scenarios, it appears that both inversion methods generally were capable of target geometry reconstruction based on apparent resistivity values, but the MLP-NN results had (by construction) sharp boundaries for the target and the Gauss-Newton results had a longer transition in resistivity at the boundary between the target and the matrix, which was attributed to the smoothing nature of the numerical solution approach. In some cases, the size of the target determined from the Gauss-Newton method was larger than the true target, and MLP-NN provided a more accurate match to the true target size (Fig. 3a and c). The rectangular shape of the target in these scenarios provides a straight-forward evaluation of the variables, whereas, since the model can capture the centroids of regular shapes, similar results are expected for irregular shapes, as well. These illustrative examples suggest that MLP-NN obtains a more accurate prediction of boundary locations and target spatial distribution, or improved reconstruction of target location geometry, as compared to Gauss-Newton inverse modeling. This improved performance of MLP-NN on the subset of scenarios as compared to Gauss-Newton method is likely due to its ability to solve non-linear, complex regression problems (Fallah et al., 2009), and numerical inverse models have accuracy limitations for locating sharp boundaries due to smoothing inherent to the numerical method. However, the least-squares method can be modified to produce a model with sharp boundaries together with a smooth resistivity

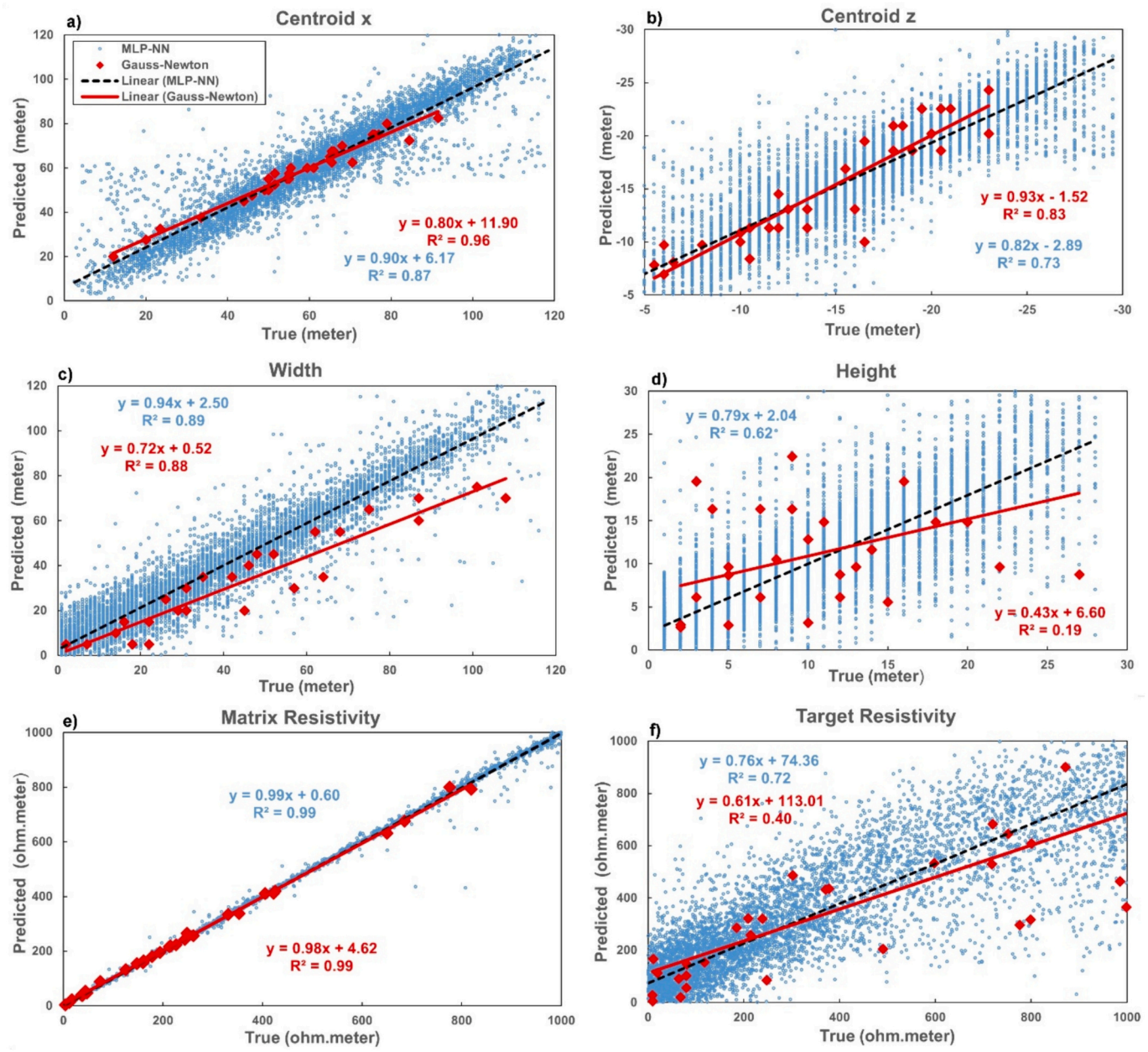

Fig. 4. Performance comparison results for Gauss-Newton and MLP-NN inversion predictions of a) 'centroid x', b) 'centroid z', c) 'target width', d) 'target height', e) 'matrix resistivity', f) 'target resistivity'.

variation, which has been used for field surveys were existence of sharp boundaries is known from engineering, geological, seismic refraction or ground-penetrating radar data (Elwaseif and Slater, 2012). In theory, it might be possible to decrease smoothing effects by employing a finer mesh in the finite-element grid, which would increase computational cost may not improve the inversion accuracy. The Gauss-Newton is also considered more effective and reliable for linear systems, but for non-linear systems, convergence slows down or may not even occur, leading to potentially unreliable parameter estimates (Huang et al., 2010).

The predictions of the six target variables, obtained with the Gauss-Newton and MLP-NN methods, are plotted versus the true values in Fig. 4. MLP-NN predictions are obtained for all 6000 samples in the testing dataset while, due to a high computational cost, Gauss-Newton predictions are only obtained for 30 samples from the dataset. In general, the data and regression results were comparable between both inversion methods for most of the six target characterization variables (see SI for regression statistics). The Gauss-Newton and MLP-NN regression lines overlap in some cases and the regression equation slope values are similar to each other, especially for 'centroid-x', 'centroid-z', and 'matrix resistivity' (Fig. 4a, b, e), which all had slope values that were approximately unity (>0.8) as a one-to-one match between prediction and the correct result. Regression slope values close to unity confirm the accuracy and lack of bias for these two inversion methods. Both Gauss-Newton and MLP-NN methods have shown promise for predictive capability of target lateral center location as 'centroid-x', vertical center as 'centroid-z', and 'matrix resistivity', which supports the application of ML for ER inversion and for mapping the location of heterogeneous structures such as, for example, subsurface karst features or perched aquifers.

The apparent increase in data scattering in both models for 'centroid-z' and 'height' (Fig. 4b and d) compared to 'centroid-x' and 'width' (Fig. 4a and c) is generally due to the differences in plot length scales (i.e., 120 m in Fig. 4a and 4c and 30 m in Fig. 4b and d). However, 'centroid-z' and 'height' (Fig. 4b and d) did have lower R^2 values, which is consistent with prior studies as target vertical position directly impacts prediction capability of ML used for ER inversion (Liu et al., 2020a). For target 'width' and 'height', the MLP-NN regression equation slope values were closer to unity compared to the Gauss-Newton method regression equation slope values (Fig. 4c and d). Plots showing a slope value <1 indicate that the Gauss-Newton had lower accuracy and increased bias (underprediction) compared to the MLP-NN method. Since the 'width' and 'height' are dependent on the target boundaries, we attribute this lower accuracy to the smoothing nature of the numerical solution approach (noted above). Fig. 4c and d results are consistent with those in Fig. 3 and confirm that MLP-NN provides a more accurate prediction of boundary locations and target spatial distribution as compared to Gauss-Newton inverse modeling. These results suggest that MLP-NN has relatively less error and prediction bias and could be preferred over the Gauss-Newton method where determination of target structure boundaries is required in practical field applications. Both inversion approaches produced highly accurate and precise predictions for 'matrix resistivity' ($R^2 > 0.98$; Fig. 4e), slope approximately one, and low data variance. Both Gauss-Newton and MLP-NN also show a linear trend in prediction of the 'target resistivity' (Fig. 4f). However, there is a high variance in predicted values, and both regression equation slopes are less than one with underprediction bias. These results indicate both methods have reduced accuracy for 'target resistivity' as compared to 'matrix resistivity', which was attributed to the smaller size of the target as compared to the entire 2D matrix. The mean target size was 396 m^2, which is a small fraction of the total 4800 m^2 for domain. Despite these limitations in prediction sensitivity, it can be inferred that MLP-NN model can be advantageous over Gauss-Newton method for approximation of 'target resistivity' in field scenarios but with lower prediction accuracy as compared to 'matrix resistivity'.

3.3. Uncertainty Quantification of Neural Network

The mean and standard deviation of each of the six target parameters were computed, and the uncertainty in the parameter estimates were represented in terms of the 95% confidence intervals. A PICP score of 0.95 was achieved for all parameters (Table 6) indicating there is 95% probability that the true responses are included within the predicted intervals and showing a confidence-consistent uncertainty quantification. Additionally, the MPIW values are similar between the training set and test set, suggesting that the ML model has reasonably learned the underlying observation-parameter relationship, and the parameter estimates for the test set can be trusted.

3.4. Application of ML models on field dataset

The field data set included ER data for multiple arrays, including the pole-pole array, that were acquired over a series of infiltration trenches (Rucker and Glaser, 2015). The trenches were designed to dispose liquid radiological waste associated with plutonium production at the U.S. DOE Hanford site in the mid-1950s. A series of eight trenches received 15×10^6 L of sodium nitrate liquid waste between 1954 and 1955 (Lindenmeier et al., 2002). Several steel cased wells were installed for geophysical well logging to detect neutron and spectral gamma emitting contaminants. In general, spectral gamma logging revealed high Cs-137 concentrations in the top 10 m of soil, and in some cases Co-60 to depths of 14 m (Rucker et al., 2013). A soil characterization borehole also revealed significant nitrate concentrations from depths 17 to 61 m below ground surface. The sodium nitrate liquid waste was the low-resistivity target for ER investigation.

The pole-pole data were converted to both Dipole-Dipole and Alt3 Wenner arrays using the procedure outlined in Rucker and Glaser (2015). The direct conversion ensured that the setup for both arrays met the input requirements for the ML input. The field data were acquired using 9 m electrode spacing, as opposed to the hypothetical model ER training data that were generated using 5 m electrode spacing. Additionally, the apparent resistivity values for field data extended beyond the hypothetical model training dataset matrix and target resistivity ranges (Data 1 of Table 2). Some of the apparent resistivity values (42 of 250) from the converted Alt3 Wenner data expanded beyond 1000 Ω.meter, which were preprocessed to 1000 Ω.meter values to be consistent with the ML model (training set range for Data 1 was 1000 Ω.meter). Therefore, MLP-NN performance was compared for 'matrix resistivity' and 'target resistivity' prediction of the testing set from Data 2 with model performance from training/testing using Data 1 (Table 2), and both training-testing sets used the constant 70:30 ratio. The primary difference was that Data 2 contained expanded matrix and target resistivity ranges including the field dataset range to evaluate MLP-NN prediction performance over the expanded ranges that included the resistivity values from the field data set (up to 5000 Ω.meter). Fig. 5 presents MLP-NN predictions of matrix resistivity and target resistivity for Data 2. These results indicated that for both parameters, predictions for the increased resistivity range were consistent with predictions obtained with the smaller resistivity ranges (Data 1) (Fig. 4e and f). Fig. 4e and 5a for the matrix were highly comparable, and Fig. 4f and 5b were

Table 6
Comparison and summary of UQ results for MLP-NN algorithm and Dipole-Dipole array combination based on Pi3nn method.

Parameter	PICP Score (Test Data)	MPIW Training Set	MPIW Test Set
Centroid x	0.95	1176.14	1194.29
Centroid z	0.95	5.52	5.56
Width	0.94	8.01	7.94
Height	0.95	3.69	3.68
Matrix Resistivity	0.95	1.25	1.23
Target Resistivity	0.95	5.53	5.52

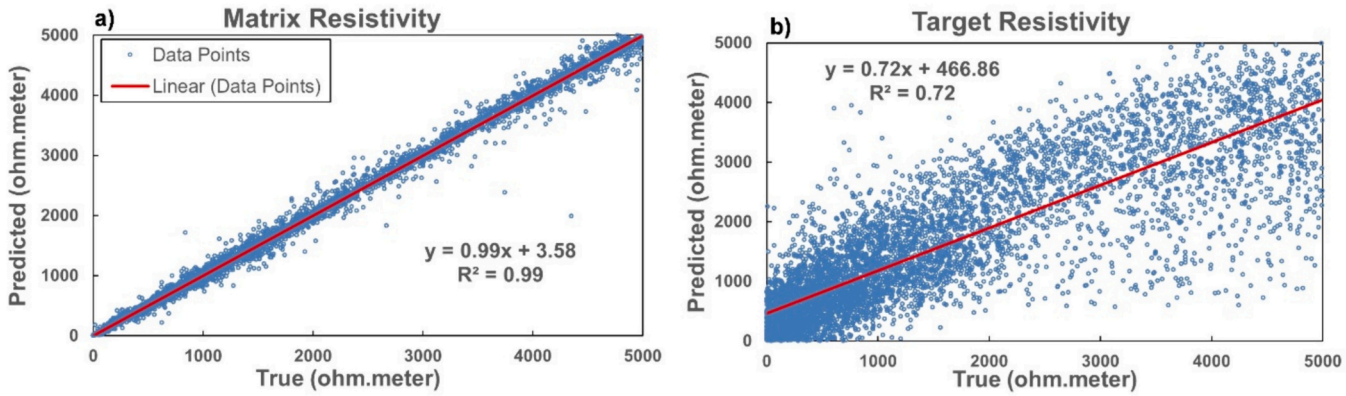

Fig. 5. MLP-NN results for prediction of a) matrix resistivity, b) target resistivity on Data 2 with expanded resistivity ranges.

also comparable for the target resistivity. Both R^2 and slope for the two parameters were closely aligned to indicate model consistency with respect to limited and expanded ranges with no significant loss in accuracy.

The field dataset was inverted using the standard Gauss-Newton inversion method (RES2DINVx64) and the MLP-NN. Fig. 6 presents Gauss-Newton results in the upper row, along with the MLP-NN results in the lower row. Results for the Dipole-Dipole and Alt3 Wenner arrays are shown in the left and right columns, correspondingly. Note that the MLP-NN Alt3 Wenner scale does not extend to 1 Ω.meter. For both ER arrays, the results shown in Fig. 6 indicate that both Gauss-Newton and MLP-NN predict similar locations and sizes for the target. It should be noted that the proposed MLP-NN method uses only six variables to describe the target and, therefore, represents any target as a rectangle with sharp boundaries. The Gauss-Newton method attempts to reconstruct the actual shape of the target, and we saw for the synthetic scenarios that the Gauss-Newton reconstruction can distort the target shape and smear its boundaries. Both lateral and vertical coordinates of the target location were more clearly identified by MLP-NN due to the sharp boundaries between target and matrix, and these findings are consistent with those discussed previously for the hypothetical scenarios (Figs. 3 and 4).

The MLP-NN and Gauss-Newton predictions of 'target resistivity' are more similar to each other for the Dipole-Dipole dataset than for Alt3 Wenner dataset, which is illustrated by the different log resistivity scale that did not extend to 1 Ω.meter for the Alt3 Wenner in the MLP-NN prediction. This result is also consistent with the trends from Table 5 for the hypothetical results. MLP-NN prediction with the Alt3 Wenner dataset was in close agreement with the Gauss-Newton predictions only for the 'matrix resistivity' out of all six target variables. Since the 'true' solution for the field dataset is unknown, it is challenging to estimate the accuracy of the two methods for this field application (measured and inverted pseudosections and % differences are in SI). The data misfit for the dipole-dipole array data set (Fig. 6) with the Gauss-Newton method is ~14.3% (Fig. S2), while the data misfit with the MLP-NN method is larger (~170%). The resistivity of the MLP-NN model rectangular model is 22.37 Ω.m while the background resistivity is 1317 Ω.m. However, the use of only six inverted variables for location characterization of a subsurface target has been shown effective for both hypothetical synthetic and field data inversions. The comparison with the Gauss-Newton method shows that the proposed MLP-NN method with six target variables can be generalized for field data to characterize the location and extent of liquid waste released at the U.S. DOE Hanford site. Specifically, MLP-NN along with Dipole-Dipole produced a reasonable match with standard numerical Gauss-Newton inversion method (Fig. S10 and S11), and the six variable target characterization approach for ML successfully locates and defines the target spatial extent with a significant reduction in amount of prediction variables compared to the prediction of the full 2D spatial distribution of resistivity properties.

These results are comparable to previously published ER inversion approaches. Some previous studies have examined numerical methods that can be used to improve identification of sharp boundaries, and as noted above there have been a few studies that used numerical inverse modeling for ER that focused on target location variables instead of full 2D domain inversion. This type of approach has been previously carried out using local (Olayinka and Yaramanci, 2000) and global (Shamara et al., 2023) nonlinear optimization methods, and these models were able to provide sharp boundaries without numerical smoothing. However, numerical inverse modeling approaches typically are dependent on neighboring values within the spatial domain, which can cause smoothing and increases computational demand. Traditional numerical inverse modeling employ optimization methods to estimate parameters through an iterative process, where computational costs escalate with the number of parameters and the nonlinearity of the model. In highly

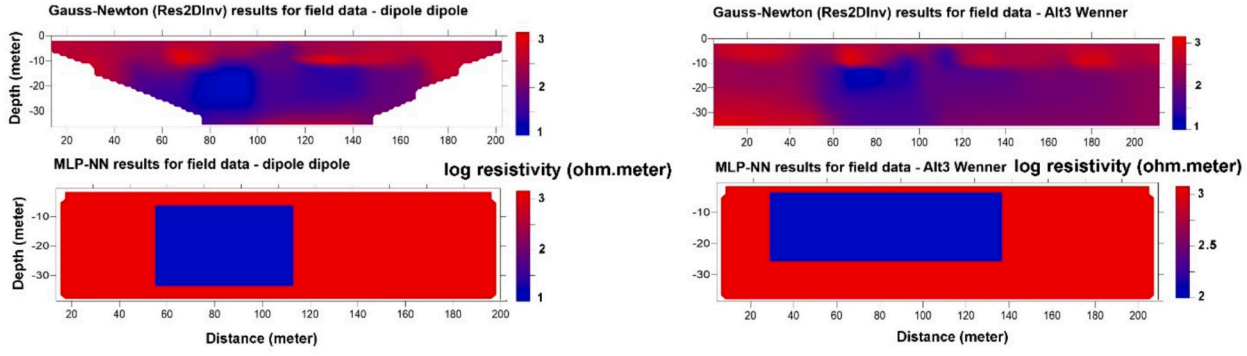

Fig. 6. MLP-NN and Gauss-Newton predictions on field dataset for dipole-dipole and Alt3 wenner array.

nonlinear problems with many parameters, a significant number of model evaluations are required to identify the optimum. Often, multiple optimization runs using different initial parameter values are necessary to avoid local optima. Computational demands for standard numerical inverse methods scale by N^3, where N is the number of unknown parameters, and the scaling limitations are mainly due to Jacobian calculations in optimization algorithms.

ML-based inverse modeling involves training a NN to learn the inverse relationship between measurable variables and unknown parameters. After the training phase, this model can quickly evaluate any given observations to produce corresponding parameter estimates. The training data for this model can be generated by running the physical model in parallel. Another way to reduce the time needed to train the ML could be through use of a semi-analytical method such as the boundary element method (Shamara et al., 2023; Xu et al., 1998). ML methods have a nearly linear scaling with N, which is achieved through efficient back-propagation algorithms. For an example that examined the inverse Darcy flow equation, the authors demonstrated this computational advantage of ML methods and their computational cost estimate included the training time (Yeung et al., 2022). Computation efficiency is further increased for ML using the six-variable target characterization approach instead of evaluating the entire 2D spatial domain. Depending on the array type and size, at least 250 ER measurements would be required for ER inversion for the entire 2D domain, and ML prediction using only the six target characterization variables is only ~2% of the variables needed for ML prediction of the 2D domain. In summary, ML-based inversion offers at least two primary advantages over traditional numerical inverse modeling:

1. Computational Efficiency: ML methods generate training data in parallel. After training, evaluations typically take just seconds. Traditional numerical inverse modeling, however, solves optimization iteratively and often requires multiple runs to mitigate local optima, with each run involving numerous iterations to achieve convergence.
2. Adaptability to New Measurements: Once an ML model has learned the inverse relationship, it can quickly produce parameter estimates for any new set of measurements without the need for re-training. Conversely, traditional numerical inverse modeling must be re-performed for each new set of measurements, adding time and complexity.

An important limitation for data-driven approaches, such as ML methods, is the potential for results to become physically infeasible. However, data-driven ML can also be used in conjunction with process-based or physics-based models, and physics informed neural networks is just one example in a growing body of research developments (Yeung et al., 2022). The ML models developed herein were trained using solutions to physics-based hypothetical models as an example approach for using process-based modeling to support ML development.

4. Conclusions

Study results confirm the feasibility of ML techniques for ER inversion for predicting the location and geometry characterization of a subsurface target zone, or anomalous body, of differing resistivity. Our unique approach constrains the ML prediction to only six target location and size characterization parameters. This approach was used to locate and define the target spatial extent while providing a significant reduction of the number of unknowns in the ER inversion (the number of discrete values of the 2D resistivity field). For the first time to the authors' knowledge, this investigation compared several ML methods over a range of ER arrays. Comparative analysis of four ML algorithms and four geophysical arrays revealed that the MLP-NN algorithm and Dipole-Dipole array combination produced the least error or highest accuracy. We found that the MLP-NN results are comparable to the traditional Gauss-Newton numerical inversion method (as the commonly used RES2DINVx64 model). Assessment of model performance indicated that both MLP-NN and Gauss-Newton numerical inversion techniques are more accurate in predicting the 'matrix resistivity' than the 'target resistivity' for the hypothetical scenarios. Both methods exhibit comparable model performance for the estimation of other target location parameters, whereas MLP-NN is more accurate than the Gauss-Newton method for estimating the target's 'width' and 'height', which was attributed to numerical smoothing in the Gauss-Newton approach. In both methods, 'centroid-z' and 'height' predictions had more error and uncertainty compared to 'centroid-x' and 'width'. This study provides quantitative confirmation of the ML and numerical method comparability, which was applied to a field data set from the U.S. DOE Hanford Site. MLP-NN predicts a sharp boundary, which is beneficial for detecting boundaries of geological layers, karst features, or foreign objects that have high resistivity contrasts. Further studies with a known ground truth are needed to estimate the comparative advantages of the MLP-NN and Gauss-Newton methods for identifying targets with naturally diffuse boundaries.

CRediT authorship contribution statement

Ahsan Jamil: Writing – original draft, Visualization, Methodology, Investigation, Formal analysis, Data curation, Conceptualization. **Dale F. Rucker:** Writing – review & editing, Writing – original draft, Validation, Supervision, Methodology, Investigation, Formal analysis, Data curation, Conceptualization. **Dan Lu:** Writing – review & editing, Validation, Software, Resources, Methodology, Investigation, Formal analysis. **Scott C. Brooks:** Writing – review & editing, Validation, Resources, Methodology, Investigation, Conceptualization. **Alexandre M. Tartakovsky:** Writing – review & editing, Validation, Methodology, Investigation. **Huiping Cao:** Writing – review & editing, Validation, Methodology, Conceptualization. **Kenneth C. Carroll:** Writing – review & editing, Writing – original draft, Validation, Supervision, Resources, Methodology, Investigation, Funding acquisition, Conceptualization.

Declaration of competing interest

The authors declare that there are no financial interests/personal relationships, which may be considered as potential competing interests.

Data availability

Supporting Information file contains statistical distributions for each parameter, ML algorithm diagrams, and linear regression statistical information. The data sets for each figure are available online at: https://figshare.com/projects/Comparison_of_Machine_Learning_and_Electrical_Resistivity_Arrays_to_Inverse_Modeling_for_Locating_and_Characterizing_Subsurface_Targets/183280

Acknowledgements

The authors are greatly appreciative of highly constructive comments from anonymous reviewers and also by the Associate Editor. This work was supported by the NSF (Award Number (FAIN): 2142686) and U.S. Department of Energy Environmental Management Minority Serving Institution Partnership Program (EM-MSIPP) managed by the Savannah River National Laboratory. Alexandre Tartakovsky was partially supported by CUSSP (Center for Understanding Subsurface Signals and Permeability), an Energy Earthshot Research Center funded by the U.S. Department of Energy (DOE), Office of Science under FWP 81834. Additional support was provided by the U.S. Department of Energy, Office of Science, Biological and Environmental Research - Research and Development Partnership Pilots (DE-SC0023132), and the Environmental System Science Research Program to the Science Focus Area (SFA) at ORNL. Oak Ridge National Laboratory is managed by UT-

Battelle, LLC, for the U.S. Department of Energy under contract DE-AC05-00OR22725.

Appendix A. Supplementary data

Supplementary data to this article can be found online at https://doi.org/10.1016/j.jappgeo.2024.105493.

References

Al Shalabi, L., Shaaban, Z., Kasasbeh, B., 2006. Data mining: a preprocessing engine. J. Comput. Sci. 2 (9), 735–739.

Aleardi, M., Vinciguerra, A., Hojat, A., 2021. A convolutional neural network approach to electrical resistivity tomography. J. Appl. Geophys. 193, 104434.

Arridge, S., Maass, P., Öktem, O., Schönlieb, C.-B., 2019. Solving inverse problems using data-driven models. Acta Numerica 28, 1–174.

Bisht, D.S., Rao, T.N., Rao, N.R., Chandrakanth, S.V., Sharma, A., 2022. Prediction of integrated water vapor using a machine learning technique. IEEE Geosci. Remote Sens. Lett. 19, 1–5.

Blanchy, G., Saneiyan, S., Boyd, J., McLachlan, P., Binley, A., 2020. ResIPy, an intuitive open source software for complex geoelectrical inversion/modeling. Comput. Geosci. 137, 104423.

Chen, T., Guestrin, C., 2016. Xgboost: a scalable tree boosting system. In: Proceedings of the 22nd acm sigkdd International Conference on Knowledge Discovery and Data Mining, pp. 785–794.

Chojnicki, K.N., Koch, J.V., Johnson, T.C., 2022. Deep Learning at Depth: Estimating Subsurface Parameters from Geophysical Monitoring Data, Pacific Northwest National Laboratory (PNNL). Richland, WA (United States).

Cubbage, B., Noonan, G.E., Rucker, D.F., 2017. A Modified Wenner Array for Efficient use of Eight-Channel Resistivity Meters. Pure Appl. Geophys. 174 (7), 2705–2718.

Dahlin, T., Leroux, V., Nissen, J., 2002. Measuring techniques in induced polarisation imaging. J. Appl. Geophys. 50 (3), 279–298.

Dey, A., Morrison, H.F., 1979. Resistivity modelling for arbitrarily shaped two-dimensional structures. Geophys. Prospect. 27 (1), 106–136.

Dong, L., Jiang, F., Wang, M., Li, X., 2022. Fuzzy deep wavelet neural network with hybrid learning algorithm: application to electrical resistivity imaging inversion. Knowl.-Based Syst. 242, 108164.

Elwaseif, M., Slater, L., 2012. Improved resistivity imaging of targets with sharp boundaries using an iterative disconnect procedure. Journal of Environmental and Engineering Geophysics 17 (2), 89–101.

Fallah, N., et al., 2009. Nonlinear Poisson regression using neural networks: a simulation study. Neural Comput. & Applic. 18, 939–943.

Gómez-Escalonilla, V., Martínez-Santos, P., Martín-Loeches, M., 2022. Preprocessing approaches in machine-learning-based groundwater potential mapping: an application to the Koulikoro and Bamako regions, Mali. Hydrology and Earth System Sciences 26 (2), 221–243.

Hayley, K., Pidlisecky, A., Bentley, L.R., 2011. Simultaneous time-lapse electrical resistivity inversion. J. Appl. Geophys. 75 (2), 401–411.

Hilbich, C., Marescot, L., Hauck, C., Loke, M.H., Mäusbacher, R., 2009. Applicability of electrical resistivity tomography monitoring to coarse blocky and ice-rich permafrost landforms. Permafr. Periglac. Process. 20 (3), 269–284.

Hiskiawan, P., Chen, C.-C., Ye, Z.-K., 2023. Processing of electrical resistivity tomography data using convolutional neural network in ERT-NET architectures. Arab. J. Geosci. 16 (10), 581.

Huang, H.-H., et al., 2010. Nonlinear regression analysis. International encyclopedia of education 2010, 339–346.

Jiang, F., Dong, L., Dai, Q., 2020. Electrical resistivity inversion based on a hybrid CCSFLA-MSVR method. Neural. Process. Lett. 51 (3), 2871–2890.

Kalliola, J., Kapočiūtė-Dzikienė, J., Damaševičius, R., 2021. Neural network hyperparameter optimization for prediction of real estate prices in Helsinki. PeerJ computer science 7, e444.

Kang, X., et al., 2018. Coupled hydrogeophysical inversion of DNAPL source zone architecture and permeability field in a 3D heterogeneous sandbox by assimilation time-lapse cross-borehole electrical resistivity data via ensemble Kalman filtering. J. Hydrol. 567, 149–164.

Karlik, B., Olgac, A.V., 2011. Performance analysis of various activation functions in generalized MLP architectures of neural networks. International Journal of Artificial Intelligence and Expert Systems 1 (4), 111–122.

Kim, Y., Nakata, N., 2018. Geophysical inversion versus machine learning in inverse problems. Lead. Edge 37 (12), 894–901.

Kosloff, D.D., Baysal, E., 1982. Forward modeling by a Fourier method. Geophysics 47 (10), 1402–1412.

Kunc, V., Kléma, J., 2024. Three Decades of Activations: A Comprehensive Survey of 400 Activation Functions for Neural Networks. arXiv preprint, arXiv:2402.09092 (2024).

LaBrecque, D.J., Ramirez, A.L., Daily, W.D., Binley, A.M., Schima, S.A., 1996. ERT monitoring of environmental remediation processes. Meas. Sci. Technol. 7 (3), 375.

Lindenmeier, C.W., et al., 2002. Characterization of vadose zone sediment: Borehole C3103 located in the 216-B-7A crib near the B tank farm. Pacific Northwest National Lab (PNNL), Richland, WA (United States).

Liu, B., et al., 2020a. Deep learning inversion of electrical resistivity data. IEEE Trans. Geosci. Remote Sens. 58 (8), 5715–5728.

Liu, B., et al., 2020b. Adaptive convolution neural networks for electrical resistivity inversion. IEEE Sensors J. 21 (2), 2055–2066.

Liu, S., Zhang, P., Lu, D., Zhang, G., 2021. PI3NN: Out-of-distribution-aware prediction intervals from three neural networks *arXiv preprint* arXiv:2108.02327.

Liu, B., Jiang, P., Guo, Q., Wang, C., 2022. Deep Learning Inversion of Electrical Resistivity Data by One-Sided Mapping. IEEE Signal Processing Letters 29, 2248–2252.

Liu, S., Lu, D., Painter, S.L., Griffiths, N.A., Pierce, E.M., 2023. Uncertainty quantification of machine learning models to improve streamflow prediction under changing climate and environmental conditions. Frontiers in Water 5, 1150126.

Loke, M.H., Barker, R.D., 1996. Rapid least-squares inversion of apparent resistivity pseudosections by a quasi-Newton method1. Geophys. Prospect. 44 (1), 131–152.

Loke, M.H., Dahlin, T., 2002. A comparison of the Gauss–Newton and quasi-Newton methods in resistivity imaging inversion. J. Appl. Geophys. 49 (3), 149–162.

Loke, M.H., Chambers, J.E., Rucker, D.F., Kuras, O., Wilkinson, P.B., 2013. Recent developments in the direct-current geoelectrical imaging method. J. Appl. Geophys. 95, 135–156.

Loke, M.H., Rucker, D.F., Chambers, J.E., Wilkinson, P.B., Kuras, O., 2020. Electrical resistivity surveys and data interpretation. In: Encyclopedia of Solid Earth Geophysics. Springer, pp. 1–6.

Olayinka, A., Yaramanci, U., 2000. Use of block inversion in the 2-D interpretation of apparent resistivity data and its comparison with smooth inversion. J. Appl. Geophys. 45 (2), 63–81.

Oliphant, T.E., 2007. Python for scientific computing. Computing in science & engineering 9 (3), 10–20.

Pang, Y., et al., 2022. 3D multi-scale resistivity inversion method applied in the tunnel face to borehole observations for tunnel-ahead prospecting. J. Appl. Geophys. 196, 104510.

Pearson, A.J., Rucker, D.F., Tsai, C.-H., Fuchs, E.H., Carroll, K.C., 2022. Electrical resistivity monitoring of lower Rio Grande River-Groundwater intermittency. J. Hydrol. 613, 128325.

Pedregosa, F., et al., 2011. Scikit-learn: machine learning in python. The Journal of Machine Learning Research 12, 2825–2830.

Pham, T.D., et al., 2020. Estimating mangrove above-ground biomass using extreme gradient boosting decision trees algorithm with fused sentinel-2 and ALOS-2 PALSAR-2 data in can Gio biosphere reserve, Vietnam. Remote Sens-Basel 12 (5), 777.

Qi, P., Zhou, W., Han, J., 2017. A method for stochastic L-BFGS optimization. 2017 IEEE 2nd International Conference on Cloud Computing and Big Data Analysis (ICCCBDA), Chengdu, 2017, pp. 156-160, doi: 10.1109/ICCCBDA.2017.7951902.

Ramchoun, H., Ghanou, Y., Ettaouil, M., Janati Idrissi, M.A., 2016. Multilayer Perceptron: Architecture Optimization and Training.

Reading, A.M., Cracknell, M.J., Bombardieri, D.J., Chalke, T., 2015. Combining machine learning and geophysical inversion for applied geophysics. ASEG Extended Abstracts 2015 (1), 1–5.

Riwayat, A.I., Nazri, M.A.A., Abidin, M.H.Z., 2018. Application of Electrical Resistivity Method (ERM) in Groundwater Exploration, Journal of Physics: Conference Series. IOP Publishing, p. 012094.

Rucker, D.F., Glaser, D.R., 2015. Standard, Random and Optimum Array Conversions from Two-pole Resistance Data. J. Environ. Eng. Geophys. 20 (3), 207–217.

Rucker, D.F., et al., 2013. Surface geophysical exploration: developing noninvasive tools to monitor past leaks around Hanford's tank farms. Environ. Monit. Assess. 185, 995–1010.

Rucker, D.F., et al., 2021a. Bedrock architecture, soil texture, and hyporheic zone characterization combining electrical resistivity and induced polarization imaging. J. Appl. Geophys. 188, 104306.

Rucker, D.F., Walker, W.K., Greenwood, J., 2021b. Three-dimensional Time-domain Induced Polarization of a Desert Aridisol for Septic Design. Journal of Environmental and Engineering Geophysics 26 (2), 153–164.

Sahu, R.K., et al., 2020. Impact of input feature selection on groundwater level prediction from a multi-layer perceptron neural network. Frontiers in Water 2.

Shamara, Z., Leticia, F., Andrés, T.A., Adrián, M., René, E., 2023. Inversion of ERT-3D data using PSO and weighting functions. J. Appl. Geophys. 215, 105091.

Sidrane, C., Katz, S., Corso, A., Kochenderfer, M.J., 2022. Verifying inverse model neural networks *arXiv preprint* arXiv:2202.02429.

Singha, K., Johnson, T.C., Day-Lewis, F.D., Slater, L., 2022. Electrical Imaging for Hydrogeology. The Groundwater Project, Guelph.

Tran, D.A., et al., 2021. Evaluating the predictive power of different machine learning algorithms for groundwater salinity prediction of multi-layer coastal aquifers in the Mekong Delta, Vietnam. Ecological Indicators 127, 107790.

Tsai, C.-H., Rucker, D.F., Brooks, S.C., Ginn, T., Carroll, K.C., 2022. Transient storage model parameter optimization using the simulated annealing method. Water Resour. Res. 58 (7) e2022WR032018.

Van Der Walt, S., Colbert, S.C., Varoquaux, G., 2011. The NumPy array: a structure for efficient numerical computation. Computing in science & engineering 13 (2), 22–30.

Vu, M.T., Jardani, A., 2021. Convolutional neural networks with SegNet architecture applied to three-dimensional tomography of subsurface electrical resistivity: CNN-3D-ERT. Geophys. J. Int. 225 (2), 1319–1331.

Wen, L., Hughes, M., 2020. Coastal wetland mapping using ensemble learning algorithms: a comparative study of bagging, boosting and stacking techniques. Remote Sens-Basel 12 (10), 1683.

Wilson, B., Singh, A., Sethi, A., 2022. Appraisal of Resistivity Inversion Models with Convolutional Variational Encoder–Decoder Network. IEEE Trans. Geosci. Remote Sens. 60, 1–10.
Xu, S.-Z., Zhao, S., Ni, Y., 1998. A boundary element method for 2-D dc resistivity modeling with a point current source. Geophysics 63 (2), 399–404.
Yeh, T.-C.J., Khaleel, R., Carroll, K.C., 2015. Flow through Heterogeneous Geologic Media. Cambridge University Press, New York.
Yeung, Y.H., Barajas-Solano, D.A., Tartakovsky, A.M., 2022. Physics-informed machine learning method for large-scale data assimilation problems. Water Resour. Res. 58 (5) e2021WR031023.